Journal of Robotics and Control (JRC)
Volume 7, Issue 3, 2026
ISSN: 2715-5072, DOI: 10.18196/jrc.v7i3.26906

Lightweight Hybrid Feature Extraction for Real-Time Skin Lesion Classification on HAM10000 and MSK10000

Fallah H. Najjar [1, 2, a, *], Farhan Mohamed [1, 3, b, *], Ali Hilal Ali [4, c], Vei Siang Chan [1, 3, d], Mohd Shafry Mohd Rahim [1, 3, e], Alfian Ma'arif [5, f], Karrar A. Kadhim [1, 6, g]
[1] Department of Emergent Computing, Faculty of Computing, Universiti Teknologi Malaysia, 81310 UTM Johor Bahru, Johor, Malaysia
[2] Department of Computer Networks and Software Techniques, Technical Institute of Najaf, Al-Furat Al-Awsat Technical University, 54001 Najaf, Iraq
[3] Media and Game Innovation Center of Excellence, Institute of Human Centered Engineering, Universiti Teknologi Malaysia, 81310 UTM Johor Bahru, Johor, Malaysia
[4] Electronic and Communications Department, Faculty of Engineering, University of Kufa, PO. Box 21, Najaf, 54001, Iraq
[5] Universitas Ahmad Dahlan, Yogyakarta, Indonesia
[6] Computer Techniques Engineering Department, Faculty of Information Technology, Imam Ja'afar Al-Sadiq University, 10001, Baghdad, Iraq
Email: [a] fallahnajjar@atu.edu.iq, [b] farhan@utm.my, [c] alih.alathari@uokufa.edu.iq, [d] vschan2@live.utm.my, [e] shafry@utm.my, [f] alfianmaarif@ee.uad.ac.id, [g] karrar.abdulameer@ijsu.edu.iq
*Corresponding Authors

***Abstract*— Skin cancer is one of the most prevalent, and in some cases deadly, cancers globally, underscoring the importance of early and precise diagnosis upon which successful disease management is dependent. Conventional diagnosis procedures are time-consuming and prone to varying routines requiring automated and consistent classification systems. In this paper, we propose a hybrid feature extraction method for binary and multi-class skin-lesion classification by integrating Local Binary Pattern (LBP) and Gray Level Run Length Matrix (GLRLM). The approach is benchmarked on two public dermoscopic image datasets (HAM10000, seven classes and MSK10000, binary classification). Twenty-one features are calculated for each image (10 LBP and 11 GLRLM), and their classification is done using five machine learning algorithms: k-Nearest Neighbor (kNN), Support Vector Machine (SVM), Decision Tree (DT), Random Forest (RF) and AdaBoost. The proposed system achieves a maximum 99.52% accuracy and a maximum 99.25% F1-score in the binary classification, outperforming many deep learning based benchmarks. In multi-class problems, it reaches 97.63% accuracy and presents high scores in precision, sensitivity, and specificity. Cross-validation verifies the stability of the model. Feature extraction requires only 0.011 seconds per image, revealing computational efficiency. Analysis of feature importance shows a consistent contribution by all the features extracted. The technique exhibits high performance, minimal computational burden, and is deployable in a real-time clinical setup. This method provides a convenient solution for early and accurate skin lesion classification in both clinical and resource-constrained environments.**

Keywords*— *Skin Cancer; Early Diagnosis; HAM10000; MSK10000; Lightweight Classification.

I. INTRODUCTION

Skin cancer is a prevalent cancer in the world [1], which has an increasing occurrence due to, for instance, augmented exposure to UV radiation and aging photo-sensitive populations [2, 3]. Early and exact diagnosis is very necessary, because treatment in time may essentially enhance the survival rate of patients [4, 5]. Dermatologists commonly perform their diagnosis based on naked eye and dermoscopic examination to detect malignant skin lesions [6-8]. However, this approach is time-consuming, subjective in nature, and it inevitably depends on inter-observer variance [9, 10]. Therefore, there has been a high demand for automatic diagnostic techniques based on medical image analysis and machine learning.

Texture-based feature extraction methods are one among such attempts, which are found to be effective in capturing the structural patterns of skin lesions [11-14]. Local Binary Pattern (LBP) and Gray Level Run Length Matrix (GLRLM) are a pair of commonly-used algorithms that measure local texture and gray-scale intensity distributions, respectively [15]. Both have been applied separately in the context of skin lesion analysis. However, their joint application in the form of a hybrid feature extraction technique for binary and multi-class classification is less investigated in the literature [16, 17]. This discrepancy becomes even clearer when we focus on lightweight and interpretable methods, appropriate for real-time exploitation on low-power devices.

Most of the existing works tend to focus on accurate deep learning models at the cost of complex computations and a lack of interpretability [18, 19]. In contrast to the existing prior art, in this study, a LBP-GLRLM hybrid feature extraction pipeline is proposed. It is expressive for achieving a balance between performance and time efficiency. We assess our approach on two widely used public datasets: the Melanoma Skin Cancer Dataset of 10000 Images (MSK10000) [20], binary classification, benign vs malignant, and the Human Against Machine dataset (HAM10000) [21], multi-class, addressing seven diagnostic categories.

Preliminary class imbalance, resolution variations, and noise in these data are rectified by data augmentation, normalization, and stratified sampling (detailed in the methodology section).

Our approach combines, implements, and evaluates a feature extraction method based on LBP and GLRLM for skin cancer classification. Our approach distinguishes itself by going beyond traditional LBP feature extraction and harnessing the potential of LBP matrix features. This innovative approach enhances the classification accuracy and provides a more comprehensive analysis of skin lesion textures, making it a valuable tool in dermatology and medical image analysis, as demonstrated in the results section. This innovative method extracts 21 features, ten from LBP and eleven from GLRLM, providing a comprehensive feature set that effectively captures skin lesions' texture and gray-scale information. Nevertheless, for the evaluation of the proposed method, five machine learning classifiers, namely k-Nearest Neighbor (kNN), Support Vector Machine (SVM), Decision Tree (DT), Random Forest (RF), and AdaBoost, have been selected to perform the classification of the extracted features.

The contributions of our method are summarized as follows:

(i) Incorporating data augmentation by rotating each image at three angles (45°, 135°, and 235°).

(ii) Extracted 21 features from skin cancer datasets using ten features from the LBP and eleven features from the GLRLM method to increase classification accuracy.

(iii) Suggested five different classifiers to classify the datasets into their corresponding classes.

(iv) Numerical results on the MSK10000 and HAM10000 datasets show that our method outperforms the state-of-the-art approaches concerning speed, accuracy, and efficiency.

The remaining sections of this paper are organized as follows: Section II will provide a thorough review of relevant literature on skin lesion classification. Section III will expound upon the proposed feature extraction method, elucidating its intricacies. Section IV will illustrate the details of the datasets. Section V will describe the experimental setup and present the results and performance analysis. Finally, Section VI will conclude the paper, underscoring its contributions and highlighting potential avenues for future research.

II. RELATED WORKS

Over the past two decades, extensive research has been conducted in Computer-Aided Diagnosis (CAD) systems to detect and identify skin cancer. Various approaches have been explored, from classical artificial intelligence to machine learning and deep learning techniques [22, 23]. Recent studies have mainly focused on employing machine learning and deep learning methods to automate melanoma detection [24].

Consequently, numerous methodologies and strategies have been proposed in published works to facilitate CAD systems. For instance, Q. U. Ain et al. conducted several studies using Genetic Programming (GP) as a feature selection method in skin cancer detection. In one study, they used GP to develop a skin cancer detection classifier by combining domain-specific features from dermatologists with LBP features from dermoscopic images. Another study introduced a method that used LBP for feature extraction, GP for feature selection, and feature engineering to enhance classification accuracy, incorporating gray-scale and color features to distinguish between benign and malignant skin lesions. They also developed a two-stage methodology for feature selection and construction using GP and LBP features from dermoscopy images [25-30].

Additionally, they created an innovative classification method using multi-tree GP to effectively distinguish between ten different skin cancer classes based on lesion images, considering both local and global information. The choice of feature extraction techniques and their integration was crucial in improving skin cancer classification performance [25-29].

İlkin et al. [31] proposed an accurate melanoma detection approach employing a hybrid classification system consisting of the SVM classifier and a bacterial colony optimization algorithm. However, this method exhibited two limitations. Firstly, the algorithm's performance deteriorated when processing images with noise, such as those containing hair or discoloration. Secondly, when the affected area extended beyond the boundaries of the image, the reliability of the classifier's features diminished.

Dhivyaa et al. [32] explored the utilization of DT and random forest classifiers for skin lesion classification. The proposed method underwent testing on the HAM10000 and ISIC 2017 datasets. Regrettably, when confronted with a large dataset, the method experiences limitations and is susceptible to image noise.

In addition, several deep learning studies were proposed to diagnose skin cancer, especially with the HAM10000 dataset; for example, Shetty et al. [33] presented a new Convolutional Neural Network (CNN) for Skin cancer classification; they used 150 epochs in the training process. Even with 150 epochs, the highest accuracy values were 95.18% and 86.43% for training and training sets, respectively. The difference in accuracy between the training and testing sets can be a sign of overfitting. In this case, the model may have learned the specific patterns in the training data but needs help generalizing them to new data.

Popescu et al. [34] introduced a multi-neural network for Skin cancer classification using nine networks with a collective intelligence block. Still, with the complexity of their proposed method, the highest accuracy was obtained at 86.71%. The main limitation of their proposed method is its high computational complexity. The nine CNNs need to be trained individually, which is computationally expensive.

Additionally, the collective intelligence block also requires a significant amount of computation. As a result, the proposed method is unsuitable for deployment on portable devices. Another area for improvement of the proposed

method is that it was only evaluated on the HAM10000 dataset. It is conceivable that the method's performance on alternative datasets may not be as satisfactory.

Shahin et al. [35] proposed an algorithm for skin cancer classification that combined two CNNs: Inception V3 and ResNet-50. The two networks were first trained individually, and then their outputs were combined using an ensemble learning method. Their proposed method achieved an accuracy of 89.90% on the HAM10000 dataset.

Finally, Srinivasu et al. [36] proposed using the MobileNet-V2 with LSTM for skin cancer classification. The MobileNet-V2 is a CNN designed to be efficient, while the LSTM is a recurrent neural network designed to learn long-term dependencies. Their proposed method achieved an accuracy of 88.90% on the HAM10000 dataset. The main limitation of their proposed method is that it needs to be sufficiently random. The input images are not randomly cropped or augmented, and the outputs of the MobileNet-V2 are not randomly shuffled, which means that the model cannot learn all possible patterns in the data.

Jadhav et al. [37] proposed a CNN to extract features of skin lesions, and an SVM was used to classify those features. The CNN was used without pre-processing for feature extraction, eliminating the need for hand-crafted features. Their proposed method achieved an accuracy of 87.25% on the HAM10000 dataset. The main limitation of their proposed method is that it is highly memory-intensive. The CNN needs to store all of the activations of the hidden layers, which can be a significant amount of data, making their proposed method challenging to deploy on devices with limited memory, such as mobile phones.

Srinivasu et al. [38] proposed a Heuristic Approach for Real-Time Image Segmentation (HARIS) for skin cancer classification. The HARIS algorithm is a two-phase algorithm that first segments the image into regions and then classifies each region. The segmentation phase uses a heuristic approach to identify the optimal number of regions in the image. The classification phase uses the SVM classifier to classify each region. Their proposed method achieved an accuracy of 84.80% on the HAM10000 dataset. Zhang et al. [39] proposed a multi-class lesion classification strategy combining the Feature Pyramid Network with Resnet-50. Their proposed approach was to train the CNN on all 1279 images from the ISBI 2016, PH2, and ISIC 2017 datasets, and then they tested it on the HAM10000 dataset. However, they stated that the obtained results for the test set of the HAM10000 dataset were 86.5%, 85.5%, 87.0%, and 86.2% for accuracy, sensitivity, precision, and F1-score, respectively. The method could be more robust to noise and variations in image quality. The Feature Pyramid Network is relatively shallow, meaning it may need help to learn to classify noisy images or have variations in image quality.

Alli et al. [40] propose an enhanced data augmentation model to detect melanoma skin cancer efficiently. Utilizing dermoscopy images from the publicly available PH2 dataset, they apply their proposed data augmentation technique to create a new skin melanoma dataset. They achieved an accuracy of 95% in binary classification, while multi-class classification yielded only 66%. However, their method could have been more effective with multi-class classification.

Bian et al. [41] proposed a deep learning-based technique for skin lesion classification that achieved promising results on three publicly available datasets. On the ISIC-2016 dataset, their model achieved an accuracy of 84.7%, a sensitivity of 64.8%, a specificity of 88.1%, and an average precision of 71.9%. On the ISIC-2017 dataset, their model achieved an accuracy of 86.2%, a sensitivity of 62.2%, and a specificity of 91.7%. On the HAM10000 dataset, their model achieved a sensitivity of 76.9% and a specificity of 96.7%. Kadry et al. [42] used a pre-trained VGG-SegNet algorithm to extract a skin melanoma region from the ISIC2016 dataset image with 224x224x3 pixels dimensions. Crucial performance parameters were determined after contrasting the extracted segmented with the ground truth. However, their proposed technique was concerned with segmentation only. However, they achieved a segmentation accuracy of 97.16%.

Nawaz et al. [43] presented a framework for melanoma segmentation that achieved a segmentation accuracy of 99% for both the ISIC-2017 and ISIC-2018 datasets. However, their method does not efficiently diagnose melanoma moles under extreme intensity variations. Their method is based on the UNet model, a CNN designed to work well on images with a relatively uniform intensity distribution. However, images of melanoma moles can have a wide range of intensity variations, making it difficult for the UNet model to segment them accurately.

In our previous works [44], a Deep Learning (DL) approach was put forth for the early detection of melanoma. This strategy incorporated a CNN network architecture featuring five convolution layers, five pooling layers, a fully connected layer, an input layer, and an output layer. Utilizing the MSK10000 dataset, the system attained an accuracy level of 91%.

Yaman et al. [45] proposed a hybrid method that fused deep feature extraction with an enhanced variant of the minimum redundancy maximum relevance (mRMR) feature selection method called ImRMR. Five pre-trained deep learning models were employed as feature generators to derive 1000 features from each model, totaling 5000 features. The ImRMR feature selection procedure was employed iteratively to automatically pick the most pertinent features, eliminating the requirement for a trial-and-error strategy. Subsequently, these chosen features were input into a Deep Neural Network (DNN) for classification. Their proposed model, presented in the study, achieved a remarkable accuracy rate of 96.58% when evaluated on the HAM10000 skin cancer image dataset.

Sharma et al. [46] investigate using machine learning and deep learning models for classifying benign and malignant skin lesions. The authors used four machine learning models: SVM, Naive Bayes (NB), kNN, and Neural Networks (NN). They also used a pre-trained SqueezeNet model for feature extraction from the MSK10000 dataset. Their study showed that the NN model outperformed the other three models in terms of accuracy, F1 measure, recall, precision, AUC, and ROC. The NN model achieved an accuracy of 88.2%, which is significantly higher than the accuracies of the other three

models (SVM: 82.4%, NB: 80.8%, kNN: 79.2%). Finally, Balaha et al. [47] proposed another deep learning approach for skin cancer detection, segmentation, and classification. Using the Harris Hawks optimization algorithm. The authors proposed optimizing five different pre-trained CNN methods: MobileNet, DenseNet201, DenseNet169, VGG19, and VGG16. Their proposed method was applied to two datasets, MSK10000 and ISIC. However, their proposed method had some restrictions. Time-consuming is the most notable advantage because it takes the longest time to train a classifier.

III. MACHINE LEARNING WORKFLOW

Whereas our study primarily focuses on traditional machine learning classifiers like kNN, SVM, DT, RF, and AdaBoost and not on neural network architectures, it is important to discuss the complexity of our approach in terms of computational cost and ease of implementation. The kNN algorithm inherently has a low model complexity as it does not involve any training phase. The primary computational cost is during the prediction phase, comparing a test instance with all training instances. However, considering the dataset sizes used in our experiments, the computation was still manageable and efficient. On the other hand, the SVM classifier is slightly more complex than kNN. It involves finding the optimal hyperplane that distinctly classifies the data points into different classes. DT involves creating a tree-like graph of decisions. The complexity of DT is relatively low and is determined by the depth of the tree. We ensured the tree depth was optimal to avoid overfitting while maintaining computational efficiency.

The LBP and GLRLM feature extraction techniques were also computationally efficient. Both techniques are known for their low computational cost and quick execution times, making them suitable for real-time applications and implementation on portable devices with limited computational resources. By focusing on these traditional classifiers and efficient feature extraction methods, our approach ensures a balance between performance and complexity, making it feasible for deployment in diverse settings, including edge devices with constrained computational capabilities.

A. Local Binary Pattern (LBP)

Ojala et al. [48] were the ones who initially presented the LBP operator. This operator works with a pixel's immediate eight neighbors, with the value of the center pixel serving as a threshold for the operation. If a neighbor pixel has the same gray value as the center pixel or a higher gray value than the center pixel, then one is assigned to that pixel. If not, then it gets a zero. Finally, the eight ones or zeros are concatenated to a binary code, resulting in the production of the LBP code for the center pixel, as shown in Fig. 1.

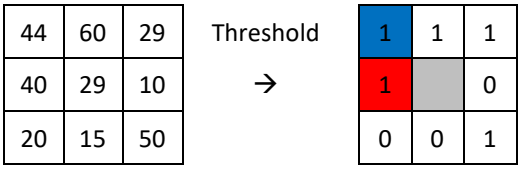

Fig. 1. LBP operator, binary: 11101001 → decimal: 233, blue: start, red: end, gray: focal pixel.

The LBP operator was later modified to accommodate a broader range of neighborhood sizes. In this case, we draw a circle with the center at pixel and radius R. The focal pixel's value is compared with readings taken from P sampling points around the circle's circumference. Any radius (R) and a different number of pixels (P) can be used to obtain the values of all nearby sampling points. The (P, R) notation is used to denote local neighborhoods. Three neighbor sets for varying values of P and R are shown in Fig. 2.

However, the modified LBP is also called extended or multiscale LBP.

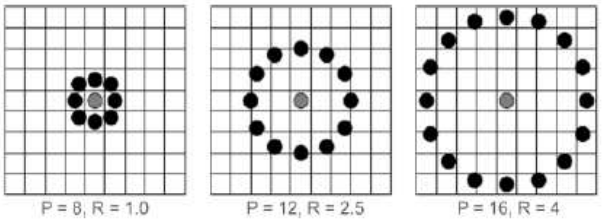

Fig. 2. Extended or multiscale LBP operator [35].

Further, the LBP feature extraction operator is denoted in Eq. 1 [48]:

$$LBP_{(P,R)} = \sum_{i=1}^{P} S(F_P - F_c)^i \qquad 1$$

Where P represents the pixel number in the neighborhood, $S(a) = 1\ if\ a \geq 0, otherwise\ 0$.

However, the LBP algorithm generates feature matrices for each image, containing ten image features [48].

TABLE I. LBP FEATURES

Features	Mathematical expression	Eq.
Contrast [49, 50]	$\sum_{r=0}^{n-1}\sum_{c=0}^{m-1}(r-c)^2 \times im(r,c)$	2
Energy [49, 50]	$\sqrt{\sum_{r=0}^{n-1}\sum_{c=0}^{m-1} im(r,c)^2}$	3
Entropy [49, 50]	$\sum_{r=0}^{n-1}\sum_{c=0}^{m-1} im(r,c) \times \log(im(r,c))$	4
Correlation [49, 50]	$\frac{1}{\sigma_r^2}\sum_{r=0}^{n-1}\sum_{c=0}^{m-1}(r-\mu_{r.})(c-\mu_{r.})\ im(r,c)$	5
Dissimilarity [49, 50]	$\sum_{r=0}^{n-1}\sum_{c=0}^{m-1}\lvert r-c\rvert\ im(r,c)$	6
Joint Variance [49, 50]	$\sum_{r=0}^{n-1}\sum_{c=0}^{m-1}(r-\mu_c)^2\ im(r,c)$	7
Joint Average [49, 50]	$\sum_{r=0}^{n-1}\sum_{c=0}^{m-1} r\ im(r,c)$	8
Cluster Prominence [49, 50]	$\sum_{r=0}^{n-1}\sum_{c=0}^{m-1}\{r-c-\mu_{p_x}\mu_{p_y}\}^4\ im(r,c)$	9
Cluster Shade [49, 50]	$\sum_{r=0}^{n-1}\sum_{c=0}^{m-1}\{r-c-\mu_{p_x}\mu_{p_y}\}^3\ im(r,c)$	10
Auto Correlation [49, 50]	$\sum_{r=0}^{n-1}\sum_{c=0}^{m-1} r\,c\ im(r,c)$	11

Table I and Table II delineate the features derived from applying LBP [48, 51-54] and GLRLM [55-57] feature extraction methodologies within the skin cancer detection system, respectively [48, 51-53].

B. Gray Level Run Length Matrix (GLRLM)

GLRLM counts the number of consecutive pixels with the same gray level value. In the GLRLM $P(r,l|\theta)$, the notation $(r,l)^2$ describes the frequency with which runs of gray level r and length l appear in the image at each angle θ.

The GLRLM is more concerned with a group of adjacent, gray-level pixels running in the same direction. GLRLM is typically calculated in four directions, with a run-length histogram for each [36, 37].

TABLE II. GLRLM FEATURES

Features	Mathematical expression	Eq.
Short Run Emphasis (SHE) [55-57]	$\frac{1}{N_z(\theta)} \times \sum_{r=1}^{N_g}\sum_{l=1}^{N_r} \frac{P(r,l\|\theta)}{j^2}$	12
Long Run Emphasis (LHE) [55-57]	$\frac{1}{N_z(\theta)} \times \sum_{r=1}^{N_g}\sum_{l=1}^{N_r} l^2 \times P(r,l\|\theta)$	13
Gray-Level Nonuniformity (GLN) [55-57]	$\frac{1}{N_z(\theta)} \times \sum_{r=1}^{N_g}(\sum_{l=1}^{N_r} \rho(r,l\|\theta))^2$	14
Run Length Nonuniformity (RLN) [55-57]	$\frac{1}{N_z(\theta)} \times \sum_{l=1}^{N_r}(\sum_{r=1}^{N_g} P(r,l\|\theta))^2$	15
Run Percentage (RP) [55-57]	$\sum_{r=1}^{N_g}\sum_{l=1}^{N_r} \frac{1}{N_p} \times P(r,l\|\theta)$	16
Low Gray Run Emphasis (LGRE) [55-57]	$\frac{1}{N_z(\theta)} \times \sum_{r=1}^{N_g}\sum_{l=1}^{N_r} \frac{P(r,l\|\theta)}{r^2}$	17
High Gray Run Emphasis (HGRE) [55-57]	$\frac{1}{N_z(\theta)} \times \sum_{r=1}^{N_g}\sum_{l=1}^{N_r} r^2 \times P(r,l\|\theta)$	18
Short Run Low Gray Emphasis (SRLGE) [55-57]	$\frac{1}{N_z(\theta)} \times \sum_{r=1}^{N_g}\sum_{l=1}^{N_r} \frac{P(r,l\|\theta)}{r^2 \times l^2}$	19
Short Run High Gray Emphasis (SRHGE) [55-57]	$\frac{1}{N_z(\theta)} \times \sum_{r=1}^{N_g}\sum_{l=1}^{N_r} \frac{P(r,l\|\theta) \times r^2}{l^2}$	20
Long Run Low Gray Emphasis (LRLGE) [55-57]	$\frac{1}{N_z(\theta)} \times \sum_{r=1}^{N_g}\sum_{l=1}^{N_r} \frac{P(r,l\|\theta) \times l^2}{r^2}$	21
Long Run High Gray Emphasis (LRHGE) [55-57]	$\frac{1}{N_z(\theta)} \sum_{r=1}^{N_g}\sum_{l=1}^{N_r} P(r,l\|\theta) \times r^2 \times l^2$	22

where: N_g represents the number of discrete intensity values in the image, N_r represents the number of discrete run lengths, N_p represents the number of voxels, $N_z(\theta)$ represents the number of runs along an angle θ, and it is equal to $\sum_{i=1}^{N_g}\sum_{j=1}^{N_r} P(r,l|\theta)$, and $1 \le N_z(\theta) \le N_p$, and $P(i,j|\theta)$ represents the normalized run length matrix $\rho(r,l|\theta) = \frac{P(r,l|\theta)}{N_z(\theta)}$.

C. Proposed method

Our proposed method comprises four stages: dataset augmentation, feature extraction, classification, and evaluation. Data augmentation is a crucial pre-processing step in our proposed method, aimed at enhancing the diversity and robustness of the dataset. In this stage, we employ a rotation-based augmentation strategy to generate additional training samples from the original dataset. The data rotation transformations expand the training data and help the model become more invariant to different orientations and viewpoints. For each input image, we apply rotation transformations at three specific angles: 45°, 135°, and 225°.

This strategy effectively simulates different orientations of the objects within the images, capturing variations that may be encountered in real-world scenarios. Introducing these augmented samples into the training set makes our model more adept at recognizing objects from different angles and can better generalize to unforeseen orientations during the testing phase. However, Table III comprehensively summarizes the hyperparameters and their corresponding values for the SVM, kNN, DT, RF, and AdaBoost classifiers.

TABLE III. HYPERPARAMETERS SUMMARIZATION

Classifier	Hyperparameter	Value
SVM	KernelFunction	Gaussian
	KernelScale	1.4
	BoxConstraint	1
	Standardize	TRUE
kNN	Cityblock	Distance
	NumNeighbors	1
	DistanceWeight	Equal
	Standardize	TRUE
DT	SplitCriterion	Deviance
	MaxNumSplits	200
	Surrogate	Off
RF	MaxNumSplits	36053
	Method	Bag
	NumLearningCycles	30
AdaBoost	MaxNumSplits	20
	Method	AdaBoostM2
	NumLearningCycles	30

Consequently, the feature extraction starts by extracting ten features using the LBP method and 11 features using the GLRLM method. We will elaborate on the details of these techniques in the following subsection. The feature extraction stage results in a feature dataset containing (42420×21) when applied to the MSK10000 dataset and (40060×21) for the HAM10000 dataset.

In order to ensure a fair comparison and to maintain consistency with our previous work, the MSK10000 dataset was randomly split into two parts: 85% for training and 15% for testing, following the division described in the referenced research paper [44]. In contrast, most cutting-edge techniques employed an 80% training and 10% testing split for the HAM10000 dataset.

Furthermore, in order to address both overfitting and bias reduction, we employed a technique known as 10-fold cross-validation. We utilized it to evaluate the performance of a model while mitigating the risks associated with overfitting

and bias. This approach divides the dataset into ten equally sized subsets or "folds" [58]. We then iteratively train the model using nine folds and evaluate its performance on the remaining fold. This process is repeated ten times, with each fold being the validation set once. Three classifiers, kNN, SVM, and DT, are trained on the training sets alongside the 10-fold cross-validation.

The performance of each classifier is evaluated using six metrics: Accuracy (Acc), Precision (Pre), Sensitivity (Sen), F1-score (F1), Specificity (Spe), and Matthews Correlation Coefficient (MCC). Fig. 3 depicts the workflow stages of this research.

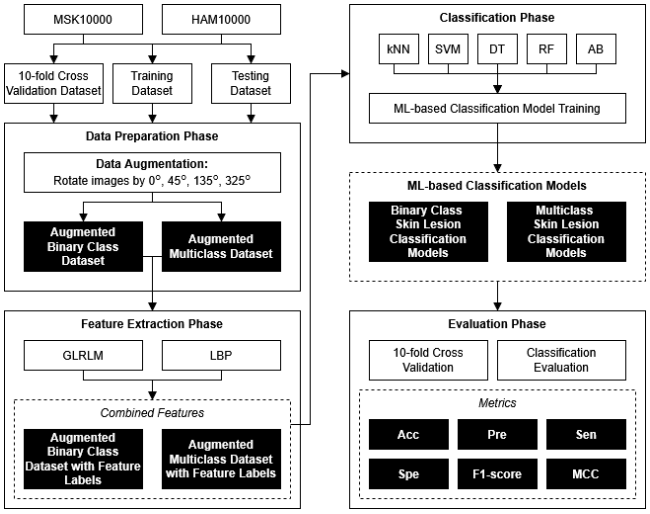

Fig. 3. Proposed workflow.

Finally, the ROC curve and AUC of the system were calculated and plotted; the ROC curve can be drawn using either class probabilities or predicted class labels. However, using predicted class labels is generally considered more informative [59].

IV. DATASETS

This section presents detailed information about the datasets employed in training the machine learning algorithms for skin cancer classification. Specifically, we utilized two datasets with distinct characteristics and significance in the field. The first dataset, MSK10000 [20], is a relatively new addition to dermatology and skin cancer research, published in 2022. Its novelty brings fresh perspectives and challenges to skin cancer classification.

On the other hand, the second dataset, HAM10000 [21], is a well-established and widely recognized dataset within the research community. It has been extensively referenced and used in numerous studies, making it a benchmark for evaluating the performance of skin cancer classification algorithms. Table IV provides a comprehensive summary of the pertinent characteristics associated with each dataset, consolidating the necessary details for easy reference.

By utilizing both MSK10000 and HAM10000 in our experiments, we aim to leverage the strengths of both datasets to develop a robust and effective skin cancer classification model that can contribute to the ongoing efforts to improve diagnostic accuracy in dermatology.

TABLE IV. MSK10000 AND HAM10000 DATASETS CLASS DISTRIBUTION

Dataset	Classes	Total images
MSK10000 [20]	benign (5500 images)	10605 (300×300)
	malignant (5105 images)	
HAM10000 [21]	melanocytic Nevi (NV) (6705 images)	10605 (600×450)
	melanoma (MEL) (1113 images)	
	benign keratosis-like lesions (BKL) (1099 images)	
	basal cell carcinoma (BCC) (514 images)	
	actinic keratoses and intraepithelial carcinoma (AKIEC) (327 images)	
	vascular lesions (VASC) (142 images)	
	dermatofibroma (DF) (115 images)	

It is clear from Table IV that the two datasets are different in terms of the number of classes. The MSK10000 has two classes [20]; therefore, it is a binary classification problem, whereas the HAM10000 has seven classes [21]. We will report the results of each dataset in the following sections.

V. EXPERIMENTAL RESULTS

Training and testing of the machine learning algorithms were performed on a local PC with Windows 11, Intel Core i7-11800H (2.30 GHz, 16 CPU), 16 GB DDR4 RAM, and NVIDIA GeForce RTX 3050 TI GPU and MATLAB (R2022a). The following section will report and discuss our results.

A. Binary Classification

In Table V, we report the experimental results of our proposed method as applied to the MSK10000 dataset. We will compare our results to the only three research efforts in the literature we found [44], [46], and [47]. In addition, kNN, SVM, DT, RF, and AdaBoost classifiers were chosen to evaluate the effectiveness of our approach. All classifiers were tested using 15% of the dataset for testing and 85% for training. Classifier efficacy is determined by comparing the classifier's predicted and actual labels. The efficacy of our proposed method was evaluated using the Acc, Pre, Spe, Sen, F1, and MCC metrics.

TABLE V. BINARY CLASSIFICATION RESULTS USING FIVE CLASSIFIERS

Metrics	kNN (%)	SVM (%)	DT (%)	RF (%)	AdaBoost (%)
Acc	99.36	99.52	99.47	99.25	98.79
Pre	99.15	99.67	99.28	99.03	98.10
Sen	99.58	99.36	99.67	99.48	99.52
F1	99.36	99.52	99.48	99.25	98.80
Spe	99.15	99.67	99.28	99.02	98.07
MCC	98.73	99.04	98.95	98.51	97.60

Table VI compares the proposed algorithm's performance with the state-of-the-art approaches to the MSK10000 dataset. Table VI shows the effectiveness of our feature extraction method in accurately classifying the skin cancer image dataset. Five different machine learning algorithms are used for classification: kNN, SVM, DT, RF, and AdaBoost. They all show results of at least 98%, suggesting outstanding performance.

TABLE VI. COMPARISON OF RESULTS WITH STATE-OF-THE-ART METHODS REGARDING THE MSK10000 DATASET

Methods	Acc (%)	Pre (%)	Sen (%)	Spe (%)
Waheed et al. [44]	91.00	-	-	-
Sharma et al. [46]	88.20	-	-	-
DenseNet169 [47]	97.08	95.38	98.65	98.50
VGG19 [47]	94.99	92.24	97.59	97.32
VGG16 [47]	94.07	92.59	95.44	94.98
MobileNet [47]	95.26	91.35	98.70	98.42
DenseNet201 [47]	96.60	95.08	97.98	97.72
Proposed (kNN)	**99.36**	**99.15**	**99.58**	**99.15**
Proposed (SVM)	**99.52**	**99.67**	**99.36**	**99.67**
Proposed (DT)	**99.47**	**99.28**	**99.67**	**99.28**
Proposed (RF)	**99.25**	**99.03**	**99.48**	**99.02**
Proposed (AdaBoost)	**98.79**	**98.10**	**99.52**	**98.07**

Table VI shows a comparison to the state-of-the-art methods in the literature. Although the approaches in the literature are primarily deep learning ones, we have shown how a more straightforward approach can be more effective with a better-suited feature extraction routine. Additionally, Fig. 4 illustrates the confusion matrix and ROC curve. Finally, the results indicate the absence of bias in the proposed method.

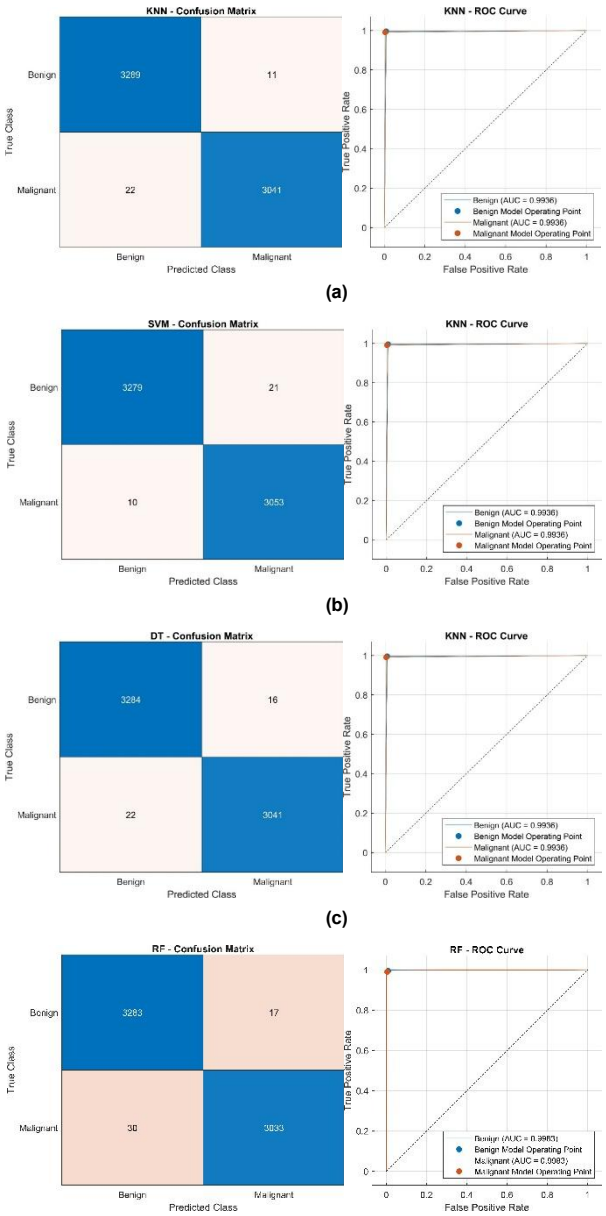

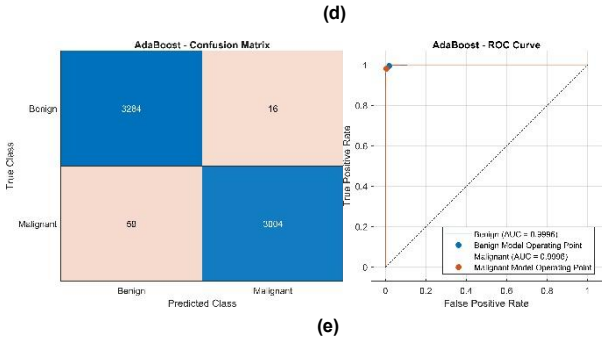

Fig. 4. Binary class confusion matrices and ROC curves: (a) kNN, (b) SVM, (c) DT, (d) RF, and (e) AdaBoost.

B. *Multi-class Classification*

In Table VII, we report our experimental results of the proposed method when applied to the HAM10000 with the same performance metrics described in previous sections.

TABLE VII. MULTI-CLASS CLASSIFICATION RESULTS USING FIVE CLASSIFIERS REGARDING THE HAM10000 DATASET

Metrics	KNN (%)	SVM (%)	DT (%)	RF (%)	AdaBoost (%)
Acc	95.86	97.63	95.71	96.80	95.03
Pre	93.17	94.40	94.49	95.08	93.42
Sen	93.16	96.56	94.14	94.70	92.80
F1	93.16	95.29	94.10	94.87	92.90
Spe	99.34	99.63	99.31	99.49	99.20
MCC	92.50	94.99	93.54	94.37	92.24

Once more, the proposed feature extraction routine has performed better in all major machine learning algorithms: SVM, kNN, DT, RF, and AdaBoost. Although the metric values are lower than the previous binary classification, we will show in Table VIII that it is better than all approaches in the literature.

TABLE VIII. COMPARISON OF RESULTS WITH STATE-OF-THE-ART METHODS REGARDING THE HAM10000 DATASET

Methods	Acc (%)	Pre (%)	Sen (%)	Spe (%)
Shetty et al. [33]	86.43	88.00	85.00	86.00
Popescu et al. [34]	86.71	-	-	-
Shahin et al. [35]	89.90	86.20	79.60	-
Srinivasu et al. [36]	85.34	-	88.24	92.00
Sönmez et al. [60]	80.79	-	-	-
Proposed (kNN)	**95.86**	**93.17**	**93.16**	**99.34**
Proposed (SVM)	**97.63**	**94.40**	**96.56**	**99.63**
Proposed (DT)	**95.71**	**94.49**	**94.14**	**99.31**
Proposed (RF)	**96.80**	**95.08**	**94.70**	**99.49**
Proposed (AdaBoost)	**95.03**	**93.42**	**92.80**	**99.20**

The highest accuracy is 97.63%, registered with the SVM algorithms equipped with our feature extraction method. It is higher by at least 10% than those in the literature. This clearly shows the versatility of the feature extraction routine even on the multi-class dataset and proves it is a strong candidate for low-computation applications such as edge devices.

Additionally, Fig. 5 introduces the multi-class confusion matrix of the classifier's test results and the system's ROC curve and AUC.

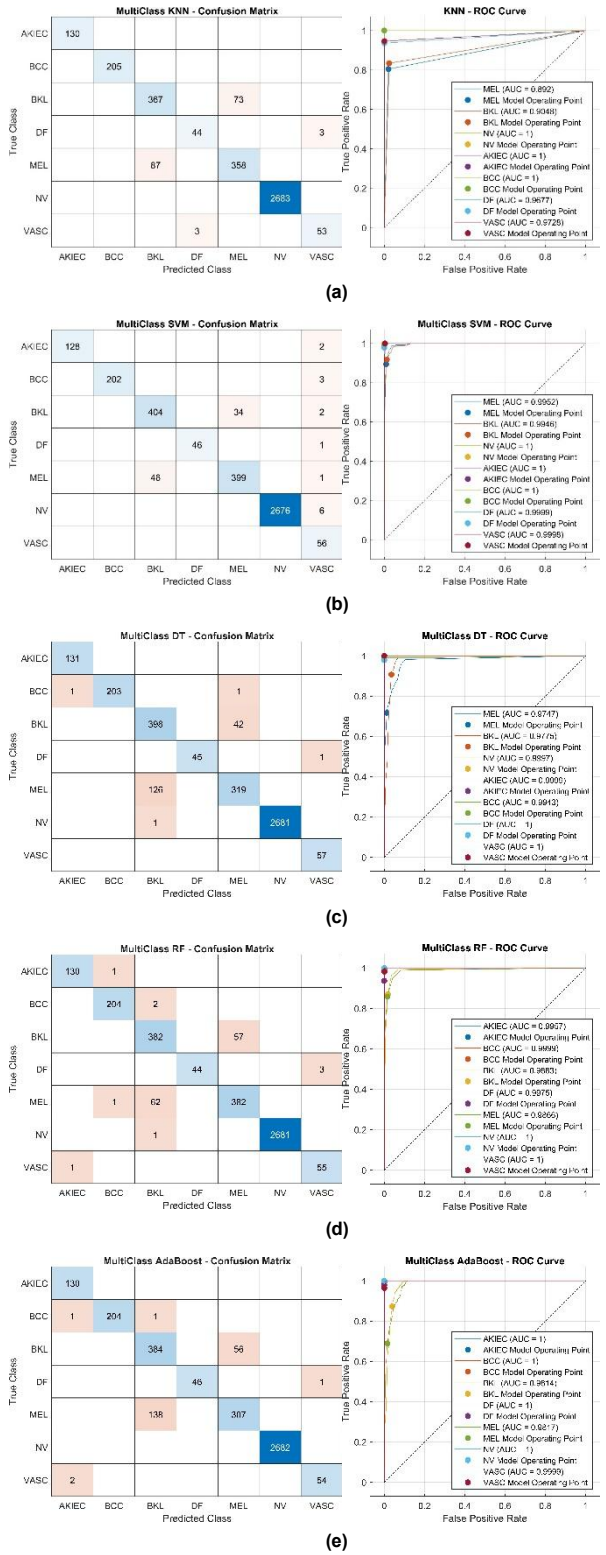

Fig. 5. Multi-class class confusion matrices and ROC curves: (a) kNN, (b) SVM, (c) DT, (d) RF, and (e) AdaBoost.

In addition, to make our classification model more interpretable and corroborate the validity of our high accuracy results, we used the feature importance function of the RF classifier. This analysis assessed the relative impact of each extracted feature, ten from LBP and eleven from GLRLM, on the final classification outcome.

Therefore, the results showed that all features were significant in the classification task, with minor variances in their importance scores. Although the features Contrast, ClusterShade, SRE, SRLGE, and SRHGE were ranked with marginally higher values, no single feature can be largely distinguished in the prediction process. However, this balanced contribution underscores the effectiveness of our hybrid feature extraction strategy.

It confirms that the selected features collectively capture a wide range of texture and gray-scale information critical for robust skin lesion classification. The feature importance plot in Fig. 6 illustrates the distribution of these values, further demonstrating that each feature adds value to the classification process.

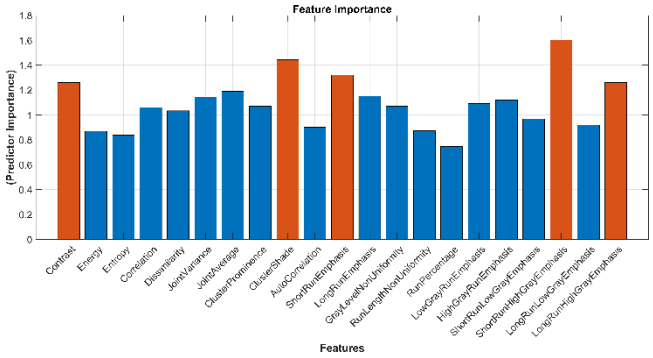

Fig. 6. Feature Importance Scores Calculated Using the RF Classifier.

C. *Cross-Validation Classification*

This section presents the results obtained from employing a technique known as 10-fold cross-validation to address the challenges of overfitting and bias. Table IX presents the binary classification results obtained from three different classifiers applied to the MSK10000 dataset using a 10-fold cross-validation technique. Table XI presents the results of multi-class classification obtained from three different classifiers.

TABLE IX. BINARY CLASSIFICATION RESULTS USING THREE CLASSIFIERS REGARDING THE MSK10000 DATASET

Metrics	KNN (%)	SVM (%)	DT (%)
Acc	99.22	99.48	98.67
Pre	98.94	99.69	98.29
Sen	99.51	99.26	99.07
F1	99.23	99.48	98.68
Spe	98.93	99.69	98.28
MCC	98.45	98.96	97.35

The results demonstrate that all three classifiers performed remarkably well on the MSK10000 dataset. The SVM classifier generally exhibited the highest scores across most metrics, indicating its superior performance in accurately classifying instances in this dataset. However, the kNN and DT classifiers also achieved high accuracy and firm performance in various evaluation measures, making them viable alternatives depending on specific requirements and preferences.

Furthermore, the Mean ± SD of performance of each classifier evaluated by 10-fold cross-validation is shown in Table X. The average F1-score was the highest for the SVM

(99.52% ± 0.16), closely followed by the DT and kNN classifiers.

TABLE X. BINARY CLASSIFICATION RESULTS USING THREE CLASSIFIERS REGARDING THE MSK10000 DATASET

Metrics	SVM (%)	kNN (%)	DT (%)
Acc	99.48 ± 0.10	99.22 ± 0.14	98.67 ± 0.31
F1	99.52 ± 0.16	99.23 ± 0.21	98.68 ± 0.28
MCC	98.96 ± 0.19	98.45 ± 0.25	97.35 ± 0.41

We performed a Wilcoxon signed-rank test for SVM vs. DenseNet169 [47] that achieved 97.08% accuracy on different scenarios. Even though our approach obtained an accuracy improvement of +2.4%, this observation was not significant ($p > 0.05$) as a result of the protocol variation. It is important to stress that our claimed superiority is situational and not an absolute one.

TABLE XI. MULTI-CLASS CLASSIFICATION DATASET

Metrics	κNN (%)	SVM (%)	DT (%)
Acc	0.9547	0.9722	0.9529
Pre	0.9367	0.9343	0.9328
Sen	0.9367	0.9559	0.9328
F1	0.9367	0.9424	0.9328
Spe	0.9927	0.9956	0.9924
MCC	0.9294	0.9392	0.9252

The results indicate that the performance of all three classifiers was commendable on the HAM10000 dataset. The SVM classifier consistently outperformed the other classifiers across most metrics, underscoring its ability to classify instances across multiple classes in this dataset accurately. Nevertheless, it is worth noting that all the kNN and DT classifiers also attained high levels of accuracy and exhibited robust performance in various evaluation measures, presenting viable alternatives that can be considered based on specific requirements and preferences.

D. Feature Extraction Period

This section will report on the feature extraction required time for each dataset in this study. Twenty-one features were extracted from each dataset. The number of samples of the MSK10000 is 42420, and 40060 samples for the HAM10000 dataset.

TABLE XII. FEATURE EXTRACTION PERIOD

Dataset	Class	#Images	Time (s)
MSK10000 300×300	Benign	5500	239.7029
	Malignant	5105	226.9732
	Total	10605	466.6761
HAM10000 600×450	NV	6705	836.1942
	BKL	1113	124.9312
	MEL	1099	118.3301
	BCC	514	58.9462
	AKIEC	327	37.7800
	VASC	142	16.0648
	DF	115	14.7922
	Total	10015	1207.0387

In the case of the MSK10000 dataset, if we divide the overall time period of the two classes by the total number of images, we will get about 0.044 seconds for each image. In the case of the HAM10000 dataset, we get about 0.1205 seconds for each image. Hence, this time represents the time required for feature extraction, including data augmentation. By dividing this number by 4, the real-time of extracting 21 features from one image is 0.011 and 0.0301 seconds for MSK10000 and HAM1000, respectively. Given the type of hardware used for conducting this experiment, our approach can be easily implemented on a budget portable hardware.

VI. CONCLUSIONS

This study suggested a novel Hybrid feature extraction method for the classification of skin lesions and incorporated both LBP, GLRLM technology. We have performed experiments using the proposed method integrated with traditional ML classifiers like SVM, kNN and Decision Tree on two publicly available datasets, MSK10000 (binary classification) and HAM10000 (multi-class classification). The system demonstrated strong performance on a variety of evaluation metrics, including an F1-score that reached 99.52% ± 0.16 for binary classification and 95.29% ± 0.94 for multi-class tasks. Moreover, the proposed method exhibited high computational efficiency that would allow for actual deployment in resource-limited scenarios.

One limitation of our study is that it focuses on applying the proposed hybrid feature extraction method and machine learning-based system on two specific datasets: HAM10000 and MSK10000. While these datasets are widely used and representative of skin cancer cases, the generalizability of our approach to other datasets or real-world clinical settings needs to be further explored and validated. Additionally, we plan to explore more sophisticated feature extraction techniques and integrate deep learning methods for further improvement. The performance and accuracy of the proposed method may vary when applied to different datasets with variations in imaging quality, demographics, and disease prevalence. The proposed method has a promising background as an effective and accurate system for classifying skin cancer. However, it will need to be more extensively validated empirically with Clinical interpretability studies and competitive benchmarking against established evaluation frameworks.

ACKNOWLEDGEMENT

This work was supported by the Universiti Teknologi Malaysia through Geran Penyelidikan Hi-Tech(F4+) with vote no.: Q.J130000.4628.00Q50.

REFERENCES

[1] R. S. Shahadh and B. Al-Khateeb, "Double dual convolutional neural network (D2CNN): A deep learning model based on feature extraction for skin cancer classification," *Iraqi Journal for Computer Science and Mathematics,* vol. 6, no. 1, p. 10, 2025.

[2] T. Ö. Varol and M. Varol, "Nanomaterials-mediated oxidative stress in cancer: recent trends and future perspectives," *Nanotherapeutics in Cancer,* pp. 97-135, 2022.

[3] N. A. Ibraheem, "Detection and Identification of Dental Caries Using Segmentation Techniques," *Ibn AL-Haitham Journal For Pure and Applied Sciences,* vol. 38, no. 3, pp. 390-406, 2025.

[4] N. Hasan *et al.*, "Skin cancer: understanding the journey of transformation from conventional to advanced treatment approaches," *Molecular cancer,* vol. 22, no. 1, p. 168, 2023.

[5] E.-G. Dobre *et al.*, "Skin cancer pathobiology at a glance: a focus on imaging techniques and their potential for improved diagnosis and surveillance in clinical cohorts," *International Journal of Molecular Sciences,* vol. 24, no. 2, p. 1079, 2023.

[6] J. Y. Chen *et al.*, "Skin cancer diagnosis by lesion, physician, and examination type: a systematic review and meta-analysis," *JAMA dermatology,* 2025.

[7] K. Harrison, "The accuracy of skin cancer detection rates with the implementation of dermoscopy among dermatology clinicians: a scoping review," *The Journal of Clinical and Aesthetic Dermatology,* vol. 17, no. 9-10 Suppl 1, p. S18, 2024.

[8] F. H. Najjar, F. Mohamed, A. N. Haidar Abdullah, M. S. Mohd Rahim, and K. A. Kadhim, "Accurate Skin Lesion Segmentation through Feature Fusion in Dermoscopy Images," *Baghdad Science Journal,* vol. 22, no. 8, 2025.

[9] M. Tran *et al.*, "Generating dermatopathology reports from gigapixel whole slide images with HistoGPT," *Nature Communications,* vol. 16, no. 1, p. 4886, 2025.

[10] F. H. Najjar, K. A. Kadhim, F. Mohamed, M. S. Mohd Rahim, and A. N. Haidar Abdullah, "A Lightweight U-Net Model for Accurate Skin Lesion Segmentation," *Iraqi Journal for Computer Science and Mathematics,* vol. 6, no. 2, p. 1, 2025.

[11] M. R. Keyvanpour, S. Vahidian, and Z. Mirzakhani, "An analytical review of texture feature extraction approaches," *International Journal of Computer Applications in Technology,* vol. 65, no. 2, pp. 118-133, 2021.

[12] P. P. Tumpa and M. A. Kabir, "An artificial neural network based detection and classification of melanoma skin cancer using hybrid texture features," *Sensors International,* vol. 2, p. 100128, 2021.

[13] Y. Vinay Kumar and H. Vimala, "Skin Cancer Classification Using PCNN-LinkNet Model Trained with Monotonic and Deep Feature Set," *Biomedical Materials & Devices,* pp. 1-33, 2025.

[14] A. A. Salam, M. U. Akram, M. H. Yousaf, and B. Rao, "DermaTransNet: Where Transformer Attention Meets U-Net for Skin Image Segmentation," *IEEE Access,* 2025.

[15] A. Bajcsi and C. Chira, "Textural and shape features for lesion classification in mammogram analysis," in *International Conference on Hybrid Artificial Intelligence Systems*, 2023: Springer, pp. 755-767.

[16] K. M. Hosny, W. M. El-Hady, F. M. Samy, E. Vrochidou, and G. A. Papakostas, "Multi-class classification of plant leaf diseases using feature fusion of deep convolutional neural network and local binary pattern," *IEEE Access,* vol. 11, pp. 62307-62317, 2023.

[17] M. S. Hossain, N. Basak, M. A. Mollah, M. Nahiduzzaman, M. Ahsan, and J. Haider, "Ensemble-based multiclass lung cancer classification using hybrid CNN-SVD feature extraction and selection method," *PLoS One,* vol. 20, no. 3, p. e0318219, 2025.

[18] A. Assis, J. Dantas, and E. Andrade, "The performance-interpretability trade-off: A comparative study of machine learning models," *Journal of Reliable Intelligent Environments,* vol. 11, no. 1, p. 1, 2025.

[19] K. A. Kadhim, O. N. Kadhim, and F. H. Najjar, "Integrating Spatial Pyramid Pooling for Multi-scale Brain Tumor Classification in Deep Learning," *Journal of Image and Graphics,* vol. 13, no. 4, 2025.

[20] M. H. Javid. Melanoma Skin Cancer Dataset of 10000 Images [Online] Available: https://www.kaggle.com/datasets/hasnainjaved/melanoma-skin-cancer-dataset-of-10000-images

[21] P. Tschandl, C. Rosendahl, and H. Kittler, "The HAM10000 dataset, a large collection of multi-source dermatoscopic images of common pigmented skin lesions," *Scientific data,* vol. 5, no. 1, pp. 1-9, 2018.

[22] T. Davenport and R. Kalakota, "The potential for artificial intelligence in healthcare," *Future healthcare journal,* vol. 6, no. 2, p. 94, 2019.

[23] J. Amin, M. Sharif, M. Raza, T. Saba, and A. Rehman, "Brain tumor classification: feature fusion," in *2019 international conference on computer and information sciences (ICCIS)*, 2019: IEEE, pp. 1-6.

[24] I. Banerjee *et al.*, "Comparative effectiveness of convolutional neural network (CNN) and recurrent neural network (RNN) architectures for radiology text report classification," *Artificial intelligence in medicine,* vol. 97, pp. 79-88, 2019.

[25] Q. U. Ain, H. Al-Sahaf, B. Xue, and M. Zhang, "Generating knowledge-guided discriminative features using genetic programming for melanoma detection," *IEEE Transactions on Emerging Topics in Computational Intelligence,* vol. 5, no. 4, pp. 554-569, 2020.

[26] Q. U. Ain, B. Xue, H. Al-Sahaf, and M. Zhang, "Genetic programming for skin cancer detection in dermoscopic images," in *2017 IEEE Congress on Evolutionary Computation (CEC)*, 2017: IEEE, pp. 2420-2427.

[27] Q. U. Ain, B. Xue, H. Al-Sahaf, and M. Zhang, "Genetic programming for feature selection and feature construction in skin cancer image classification," in *PRICAI 2018: Trends in Artificial Intelligence: 15th Pacific Rim International Conference on Artificial Intelligence, Nanjing, China, August 28–31, 2018, Proceedings, Part I 15*, 2018: Springer, pp. 732-745.

[28] Q. U. Ain, B. Xue, H. Al-Sahaf, and M. Zhang, "Multi-tree genetic programming with a new fitness function for melanoma detection," in *2019 IEEE Congress on Evolutionary Computation (CEC)*, 2019: IEEE, pp. 880-887.

[29] Q. U. Ain, B. Xue, H. Al-Sahaf, and M. Zhang, "Genetic programming for multiple feature construction in skin cancer image classification," in *2019 International Conference on Image and Vision Computing New Zealand (IVCNZ)*, 2019: IEEE, pp. 1-6.

[30] F. H. Najjar, S. Abd Kadum, and N. B. Hassan, "Integrating Multi-scale Feature Extraction into EfficientNet for Acute Lymphoblastic Leukemia Classification," *Journal of Image and Graphics,* vol. 13, no. 1, pp. 83-89, 2025.

[31] S. İlkin, T. H. Gençtürk, F. K. Gülağız, H. Özcan, M. A. Altuncu, and S. Şahin, "hybSVM: bacterial colony optimization algorithm based SVM for malignant melanoma detection," *Engineering Science and Technology, an International Journal,* vol. 24, no. 5, pp. 1059-1071, 2021.

[32] C. Dhivyaa, K. Sangeetha, M. Balamurugan, S. Amaran, T. Vetriselvi, and P. Johnpaul, "Skin lesion classification using decision trees and random forest algorithms," *Journal of Ambient Intelligence and Humanized Computing,* pp. 1-13, 2020.

[33] B. Shetty, R. Fernandes, A. P. Rodrigues, and K. Lakshmanna, "Skin Lesion Classification of Dermoscopic Imagesusing Machine Learning and Convolutional Neural Network," *Sci Rep,* vol. 12, p. 18134 2022.

[34] D. Popescu, M. El-Khatib, and L. Ichim, "Skin Lesion Classification Using Collective Intelligence of Multiple Neural Networks," *Sensors,* vol. 22, no. 12, p. 4399, 2022.

[35] A. H. Shahin, A. Kamal, and M. A. Elattar, "Deep ensemble learning for skin lesion classification from dermoscopic images," in *2018 9th Cairo International Biomedical Engineering Conference (CIBEC)*, 2018: IEEE, pp. 150-153.

[36] P. N. Srinivasu, J. G. SivaSai, M. F. Ijaz, A. K. Bhoi, W. Kim, and J. J. Kang, "Classification of skin disease using deep learning neural networks with MobileNet V2 and LSTM," *Sensors,* vol. 21, no. 8, p. 2852, 2021.

[37] A. R. Jadhav, A. G. Ghontale, and V. K. Shrivastava, "Segmentation and border detection of melanoma lesions using convolutional neural network and SVM," in *Computational Intelligence: Theories, Applications and Future Directions-Volume I*: Springer, 2019, pp. 97-108.

[38] P. N. Srinivasu, T. S. Rao, and V. E. Balas, "A systematic approach for identification of tumor regions in the human brain through HARIS algorithm," in *Deep Learning Techniques for Biomedical and Health Informatics*: Elsevier, 2020, pp. 97-118.

[39] M. A. Khan, Y.-D. Zhang, M. Sharif, and T. Akram, "Pixels to classes: intelligent learning framework for multiclass skin lesion localization and classification," *Computers & Electrical Engineering,* vol. 90, p. 106956, 2021.

[40] O. O. Abayomi-Alli, R. Damasevicius, S. Misra, R. Maskeliunas, and A. Abayomi-Alli, "Malignant skin melanoma detection using image augmentation by oversamplingin nonlinear lower-dimensional embedding manifold," *Turkish Journal of Electrical Engineering and Computer Sciences,* vol. 29, no. 8, pp. 2600-2614, 2021.

[41] J. Bian, S. Zhang, S. Wang, J. Zhang, and J. Guo, "Skin lesion classification by multi-view filtered transfer learning," *IEEE Access,* vol. 9, pp. 66052-66061, 2021.

[42] S. Kadry, D. Taniar, R. Damaševičius, V. Rajinikanth, and I. A. Lawal, "Extraction of abnormal skin lesion from dermoscopy image using VGG-SegNet," in *2021 Seventh International conference on Bio Signals, Images, and Instrumentation (ICBSII)*, 2021: IEEE, pp. 1-5.

[43] M. Nawaz *et al.*, "Melanoma segmentation: A framework of improved DenseNet77 and UNET convolutional neural network," *International Journal of Imaging Systems and Technology,* vol. 32, no. 6, pp. 2137-2153, 2022.

[44] S. R. Waheed *et al.*, "Melanoma Skin Cancer Classification based on CNN Deep Learning Algorithms," *Malaysian Journal of Fundamental and Applied Sciences,* vol. 19, no. 3, pp. 299-305, 2023.

[45] O. Yaman, S. Dogan, T. Tuncer, and A. Subasi, "Skin cancer classification model based on hybrid deep feature generation and iterative mRMR," in *Computational Intelligence Based Solutions for Vision Systems*: IOP Publishing Bristol, UK, 2022, pp. 4-1-4-24.

[46] S. Sharma, K. Guleria, S. Kumar, and S. Tiwari, "Benign and Malignant Skin Lesion Detection from Melanoma Skin Cancer

Images," in *2023 International Conference for Advancement in Technology (ICONAT)*, 2023: IEEE, pp. 1-6.

[47] H. M. Balaha, A. E.-S. Hassan, E. M. El-Gendy, H. ZainEldin, and M. M. Saafan, "An Aseptic Approach Towards Skin Lesion Localization and Grading using Deep Learning and Harris Hawks Optimization," *Research Square,* 2022.

[48] T. Ojala, M. Pietikäinen, and D. Harwood, "A comparative study of texture measures with classification based on featured distributions," *Pattern recognition,* vol. 29, no. 1, pp. 51-59, 1996.

[49] F. H. Najjar, K. A. Kadhim, M. H. Kareem, H. A. Salman, D. A. Mahdi, and H. M. Al-Hindawi, "Classification of COVID-19 from X-ray Images using GLCM Features and Machine Learning," *Malaysian Journal of Fundamental and Applied Sciences,* vol. 19, no. 3, pp. 389-398, 2023.

[50] F. H. Najjar, H. M. Al-Jawahry, M. S. Al-Khaffaf, and A. T. Al-Hasani, "A novel hybrid feature extraction method using LTP, TFCM, and GLCM," in *journal of physics: conference series*, 2021, vol. 1892, no. 1: IOP Publishing, p. 012018.

[51] J. Liu, M. Jin, N. Sun, G. Han, and S. Kwong, "Correlation statistical modeling between visual privacy-protection evaluation and human-pose recognition," *Measurement,* vol. 184, p. 109942, 2021.

[52] L. Nanni, A. Lumini, and S. Brahnam, "Survey on LBP based texture descriptors for image classification," *Expert Systems with Applications,* vol. 39, no. 3, pp. 3634-3641, 2012.

[53] T. Ojala, M. Pietikainen, and T. Maenpaa, "Multiresolution gray-scale and rotation invariant texture classification with local binary patterns," *IEEE Transactions on pattern analysis and machine intelligence,* vol. 24, no. 7, pp. 971-987, 2002.

[54] Ş. Öztürk and B. Akdemir, "Application of feature extraction and classification methods for histopathological image using GLCM, LBP, LBGLCM, GLRLM and SFTA," *Procedia computer science,* vol. 132, pp. 40-46, 2018.

[55] H. Zhang, C.-L. Hung, G. Min, J.-P. Guo, M. Liu, and X. Hu, "GPU-accelerated GLRLM algorithm for feature extraction of MRI," *Scientific reports,* vol. 9, no. 1, pp. 1-13, 2019.

[56] M. K. Ghalati, A. Nunes, H. Ferreira, P. Serranho, and R. Bernardes, "Texture analysis and its applications in biomedical imaging: A survey," *IEEE Reviews in Biomedical Engineering,* 2021.

[57] R. W. Conners and C. A. Harlow, "A theoretical comparison of texture algorithms," *IEEE transactions on pattern analysis and machine intelligence,* no. 3, pp. 204-222, 1980.

[58] A. A. Mir *et al.*, "Anomalies prediction in radon time series for earthquake likelihood using machine learning-based ensemble model," *IEEE Access,* vol. 10, pp. 37984-37999, 2022.

[59] A. Tharwat, "Classification assessment methods," *Applied computing and informatics,* vol. 17, no. 1, pp. 168-192, 2020.

[60] A. F. SÖNMEZ, S. ÇAKAR, F. CEREZCİ, M. KOTAN, İ. DELİBAŞOĞLU, and Ç. Gülüzar, "Deep Learning-Based Classification of Dermoscopic Images for Skin Lesions," *Sakarya University Journal of Computer and Information Sciences,* vol. 6, no. 2, pp. 114-122, 2023.